[Short title + Author Name - P&H title] 17 (2024) 105694

Contents lists available at ScienceDirect

Arabian Journal of Chemistry

journal homepage: www.ksu.edu.sa

# Synthesized tin oxide nanoparticles promote apoptosis in human osteosarcoma cells

Ruxin Ruan [1], Rui Chen [1], Huaixi Yu [*]

*Department of Orthopedics, The Affiliated Huai'an Hospital of Xuzhou Medical University, Huai'an Second People's Hospital, Huai'an, Jiangsu, China*

ARTICLE INFO

*Keywords:*
Tin oxide
Nanoparticle
Characterization
Apoptosis
Osteosarcoma

ABSTRACT

Complicated protocols have been used to tune the size of tin oxide nanoparticles ($SnO_2$ NPs) in conventional chemical synthesis approaches. In this study, we addressed this issue through the combination of polarity solvent reduction and sonication as a potential strategy for optimizing the size of $SnO_2$ NPs for anticancer applications. Then the anticancer activity and safety of synthesized $SnO_2$ NPs on U-2OS human osteosarcoma cells and normal human osteoblast, NHOst, respectively, were assessed by several assays. SEM and TEM analyses revealed that synthesized $SnO_2$ NPs had a spherical-shaped morphology with an average particle size of about 10 nm. FTIR result showed a broad absorption peak at 649 $cm^{-1}$, corresponding to the stretching vibration of the O–Sn–O bond. XRD analysis exhibited eight main peaks, revealing a tetragonal system of rutile-like structure. DLS study showed that synthesized $SnO_2$ NPs had an average hydrodynamic size of 43.93 nm with a zeta potential value of −31.00 mV. Cellular assays displayed that $SnO_2$ NPs mitigate the growth of U-2OS human osteosarcoma cells ($IC_{50}$: 15.50 μg/mL) with partial cytotoxicity on normal osteoblasts. It was then discovered that $SnO_2$ NPs triggered stress effects by raising the levels of LDH release, ROS, and MDA and lowering those of SOD, CAT activity, and GSH content. Also, it was discovered that $SnO_2$ NPs activated both intrinsic and extrinsic signaling pathways mediated by MMP collapse, elevation of caspase-3, −9, −8 activities and corresponding mRNA, and upregulation of Bax/Bcl-2 mRNA ratio. Overall, this study found that extrinsic and mitochondrial apoptotic pathways can both be activated by synthesized $SnO_2$ NPs to induce apoptosis in human osteosarcoma cells. This finding calls for additional research in the future.

## 1. Introduction

The most prevalent type of primary solid bone tumor, osteosarcoma, is recognized by the existence of malignant mesenchymal cells that generate osteoid as well as immature bone. In adolescence, 15 % of all solid extracranial cancers are osteosarcomas and males typically experience this disorder 1.4 times more often than females. The promising treatment of patients suffering from osteosarcoma requires multidisciplinary supervision (Ritter and Bielack, 2010).

The capability of nanotechnology to improve the early detection, diagnostics, and therapeutic approaches of different cancer cells has recently received overwhelming attention (Ferrari, 2005). Therefore, the application of new strategies that benefit from nanotechnology may open new avenues in the prevention and treatment of osteosarcoma (Alrushaid et al., 2023).

The synthesis of inorganic nanoparticles (NPs) with prominent biomedical characteristics is a crucial challenge and has recently obtained enormous interest (Tuli,Joshi,et al., 2023).

Sonochemistry is known as one of the earliest strategies utilized to prepare nanostructured materials. In this technique, particles go through a chemical reaction following exposure to strong ultrasound radiation (20 kHz–10 MHz) which results in an acoustic cavitation sonochemical process. In comparison with other conventional approaches, the sonochemical method results in the production of NPs with more uniform dispersity, a higher surface area, higher thermal stability, and better phase purity (Low et al., 2022). However, it should be noted that this method needs highly controllable protocols to result in the synthesis of monodisperse NPs with desirable dimensions (Li et al., 2021). Also, surface modification of NPs with different moieties is complicated due to the hydrophobicity of the organic ligands in water. Therefore, much attention has been given to addressing these drawbacks of the sonochemical method by controlling the solvent polarity (Hussain

* Corresponding author.
*E-mail address:* 15152353021@163.com (H. Yu).
[1] Ruxin Ruan and Rui Chen contributed equally to this work and should be considered co-first authors.

https://doi.org/10.1016/j.arabjc.2024.105694
Received 23 January 2024; Accepted 23 February 2024
Available online 25 February 2024

et al., 2020). Therefore, in this paper, we used a combination route for the synthesis of NPs via sonochemical method along with the application of a mixture of water and ethanol for the reduction of the polarity of water as a solvent.

Owing to the elegant biomedical features of metal oxides, they have been using as a future potential stone in cancer therapy through the induction of apoptosis (Shabatina et al., 2023; Saini et al., 2016; Bandyopadhyay et al., 2020). Pure metal oxide of tin oxide ($SnO_2$) has shown promising anticancer activities on a wide range of cancers, including ovarian (Hanna and R. Saad 2021), blood (Ahmadabad et al., 2021), and breast cancer cells (Guo et al., 2021). Hanna et al. showed that $SnO_2$ NPs could induce mitochondria-mediated apoptosis in ovarian cancer cells (Hanna and R. Saad 2021). Also, Ahamed et al. reported that reactive oxygen species (ROS)-mediated apoptosis could be the anticancer mechanism of $SnO_2$ NPs in breast cancer cells (Ahamed et al., 2018).

Though many studies have been published on the anticancer activity of $SnO_2$ NPs, selective apoptosis induction of $SnO_2$ NPs on different types of cancer cells *in vitro* was not well-explored. As osteosarcoma is one of the most common primary malignant bone tumors and occurs mainly in childhood and young adults, the selective apoptosis induction in these types of tumors could be considered as a promising strategy in modulation of this disorder. Therefore, the main aim of this study was to assess the anticancer effects of $SnO_2$ NPs synthesized through a combination method (sonochemical along with solvent polarity reduction) on U-2OS human osteosarcoma cells.

## 2. Materials and methods

### 2.1. Materials

Tin(II) chloride dehydrate ($SnCl_2{\cdot}2H_2O$, ACS reagent, 98 %, product No. 243523), 2, 7-dichlorofluorescein diacetate (DCFDA), and Dulbecco's Modified Eagle's Medium (DMEM) were purchased from Sigma (St. Louis, MO, USA). Fetal bovine serum (FBS) and antibiotics were purchased from Invitrogen (Carlsbad, CA, USA).

### 2.2. Synthesis of $SnO_2$ NPs through combination method

$SnCl_2{\cdot}2H_2O$ (Merck) (1 M) suspended in 100 mL water–ethanol mixture (10 % ethanol, to reduce the polarity of water solvent) were stirred (500 rpm for 30 min) followed by irradiation by a high intensity ultrasonic processor (750 W; 20 kHz and 6 mm Ti-probe tip) for 1 h. The pH of the medium was regulated by ammonium hydroxide (Sigma Aldrich) and gradually added to reach a range between 9 and 10 to result in the formation of monodispersed NPs. The temperature was also set at 80–90 °C during the sonication system. The samples were then centrifuged (5 min, 3000 rpm/min), washed several times with deionized water, dried at 70℃, and finally calcined at 500℃ for 2 h (Rehman et al., 2020).

### 2.3. Characterization of the synthesized $SnO_2$ NPs

The particle size and the morphological structure were investigated by transmission electron microscope TEM (FEI Tecnai G2 X-TWIN 100 kV) and scanning electron microscope (SEM, MIRA3). Fourier transform infrared (FTIR) was done on a spectrophotometer (FTIR- Tensor 27, Bruker, Germany) in the range of 4000–400 $cm^{-1}$). Phase identification and crystalline nature of the synthesized $SnO_2$ NPs were measured by X-ray diffraction (XRD) using a diffractometer system (PANalyticalX'pert PRO XRD), Cu as anodic materials [CuKα radiation (λ = 1.54178 Å), 40 kV and 30 mA] with scan step in 2θ range from 20° to 80°. The hydrodynamic radius and zeta potential distribution of $SnO_2$ NPs were measured using dynamic light scattering (DLS, Malvern Instruments, Worcestershire, UK, ZEN 3600 model Nano ZS).

### 2.4. Cell culture

Human osteosarcoma, U-2OS, and normal human osteoblast, NHOst, cell lines obtained from American Type Culture Collection (ATCC, Manassas, VA, USA), were cultured in DMEM supplemented with 10 % FBS, 1 % antibiotics, 1 mM L-glutamine (Gibco, Grand Island, NY, USA) and 100 μg/mL gentamicin (Gibco, Grand Island, NY, USA) at 37 °C with 5 % $CO_2$.

### 2.5. Cell viability assay

Cell viability assay was done using a conventional MTT assay. Briefly, cancerous and noncancerous cells seeded into 96-well culture plates with a density of $5 \times 10^3$ cells/well were incubated for 24 h. Afterward, $SnO_2$ NPs with different concentrations ranging from 1 to 100 μg/mL were transferred and further incubated for 24 h. Then, 50 μl of MTT (5 mg/mL) was added into each well after removing the culture medium and incubated for 4 h at 37 °C. 100 μl of dimethyl sulfoxide was then added to the wells and the optical density (OD) of the solution was detected at 570 nm on a microplate ELISA reader.

### 2.6. Lactate dehydrogenase (LDH) release assay

LDH assay was used to evaluate the cytotoxic effects of $SnO_2$ NPs on U-2OS human osteosarcoma cells or NHOst normal cells. Cells seeded in a 96-well plate at a density of $5 \times 10^3$ cells/well were exposed to $IC_{50}$ concentration of $SnO_2$ NPs (15.50 μg/mL) for 24 h. LDH Assay Kit (Shanghai Biyuntian Biotechnology Co., Ltd.) was used to detect the LDH release in cell culture medium according to the manufacturer's protocol and the absorbance of the sample was read at 490 nm using a microplate ELISA reader.

### 2.7. Reactive oxygen species analysis (ROS)

ROS assay was used to assess the oxidative stress induced by $SnO_2$ NPs in U-2OS human osteosarcoma cells. Cells seeded in a 6-well plate at a density of $3 \times 10^5$ cells/well were incubated with $IC_{50}$ concentration of $SnO_2$ NPs (15.50 μg/mL) for 6 h. Afterward, cells were collected, washed, and suspended in a DCFH-DA solution (20 μM) for 30 min. The cells were then washed and the fluorescence intensity of fluorescent product 2′,7′-dichlorofluorescein (DCF) was read on a SYNERGY-HT multiwell plate reader, Bio-Tek (USA) at excitation and emission wavelengths of 485 and 528 nm, respectively.

### 2.8. Oxidative stress analysis

Cells with a density of ~$5 \times 10^6$ in a 75 $cm^2$ culture flask exposed to $IC_{50}$ concentration of $SnO_2$ NPs (15.50 μg/mL) were scraped, washed with chilled 1 × PBS, and centrifuged at 500g for 15 min. The pellets were washed and then incubated on ice with 1 × Lysis Buffer (10 mM Tris, pH 7.5, 150 mM NaCl, 0.1 mM EDTA, 0.5 % Triton-100) for 10 min supplemented with appropriate protease inhibitors. Then, the cells were centrifuged at 12 000 g for 10 min and the supernatant was collected. Protein concentration was determined by the Bradford assay (Bonjoch and Tamayo, 2001). Subsequently, superoxide dismutase (SOD, A001-1; Nanjing Jiancheng Bioengineering Institute) and catalase (CAT, A007-2; Nanjing Jiancheng Bioengineering Institute) activities as well as glutathione (GSH, A006-1; Nanjing Jiancheng Bioengineering Institute) and 3,4-Methylenedioxyamphetamine (MDA, A003-1; Nanjing Jiancheng Bioengineering Institute) contents were detected with relevant detection kits according to the protocols recommended by the manufacturer.

### 2.9. Activity of caspase-3, caspase-9, and caspase-8

The activity levels of caspase-3, caspase-9 and caspase-3 were measured according to the manufacturer's protocol provided with the

caspase colorimetric assay kits (Nanjing Jiancheng Bioengineering Institute). Briefly, an aliquot of cell suspension was mixed with the reaction buffers containing the substrates followed by incubating at 37 °C for 2 h and terminating by the addition of a stop buffer. Then, the optical density of samples was read at 405 nm using a microplate ELISA reader.

### 2.10. Mitochondrial membrane potential (MMP)

Cells were seeded in a 6-well microculture plate at a density of $3 \times 10^5$ cells/well and after incubation with $IC_{50}$ concentration of $SnO_2$ NPs (15.50 μg/mL) for 24 h, then the medium was replaced with reaction buffer provided with MMP kit (Shanghai Yeasen Biotechnology Co., Ltd.). The relative ratio of red to green fluorescence intensity was determined as the level of MMP depolarization.

### 2.11. Total RNA extraction and quantitative real-time PCR (qRT-PCR)

Cells were seeded in a 6-well microculture plate at a density of $3 \times 10^5$ cells/well and after incubation with $IC_{50}$ concentration of $SnO_2$ NPs (15.50 μg/mL) for 24 h total RNA was extracted by RNA isolation Kit (Huayueyang Biotechnology, China) according to the manufacturer's instructions. After checking the quantity and quality of RNA, the cDNA synthesis kit (Takara, Beijing, China) was used to reverse-transcribe RNA following the manufacturer's instructions. The reactions were done on a Bio-red IQ2 Sequence Detection System and Applied Biosystems software using SYBR Green PCR Master Mix (Applied Biosystems) following the standard protocols. Primer design was based on previous studies (Liang et al., 2012; Punzo et al., 2017). The comparative threshold cycle (Ct) values were calculated and analyzed using the $2^{-\Delta\Delta CT}$ method, with β-actin as an internal control.

### 2.12. Statistics analysis

SPSS statistics package was used for statistical analysis between different groups by one-way analysis of variance (*$P < 0.05$, ** $P < 0.01$, *** $P < 0.001$).

## 3. Result and discussion

### 3.1. Imaging analysis

SEM and TEM analyses were done to determine the shape and size of the synthesized $SnO_2$ NPs. The morphology of $SnO_2$ NPs was assessed, whereas the size of NPs was determined by the TEM test. SEM images showed that synthesized $SnO_2$ NPs provided monodispersed spherical-or quasi-spherical-shaped morphology (Fig. 1A). TEM analysis revealed that synthesized $SnO_2$ NPs show the average particle size around 10 nm (Fig. 1B). In other words, from TEM analysis, the probable uniform distribution of small sized $SnO_2$ NPs (about 10 nm) is revealed. This can be attributed to the cavitational effects stimulated by ultrasound, which results in the generation of extreme shearing forces, micromixing and turbulence derived from physical influences inserted by the transient deformation of cavities that appeared due to ultrasound (Deosarkar et al., 2013; Choudhari et al., 2020; Karunakaran,Raadha,and Gomathisankar, 2013). Also, solvent polarity reduction not only results in the dispersion of synthesized NPs but also a decrease in the size of NPs (Hussain et al., 2020).

Sery et al. (Sery et al., 2022) reported that synthesized $SnO_2$ NPs through the sonochemical method had a wide size range of 2 to 30 nm, which makes them complicated for biological applications Karunakaran et al. (Karunakaran,Raadha,and Gomathisankar, 2013) also showed that sonochemically synthesized $SnO_2$ NPs had an average diameter of 10 nm, which is in good agreement with our TEM result. However, they found that the prepared NPs lack finite shape or structure, which might be due to the generation of hotspots through the sonochemical method as the main destructors of the templating effect. Additionally, Zhu et al. reported that sonochemically synthesized $SnO_2$ NPs in an aqueous solution of $SnCl_4$ and azodicarbonamide were ~3 – 5 nm in size, as detected by TEM analysis (Zhu et al., 2000). However, it should be indicated that ultrasmall NPs (around 3 to 5 nm) are easily filtered by liver and kidney tissues. Therefore, we can conclude that sonochemistry along with solvent polarity reduction could result in the synthesis of $SnO_2$ NPs with monodispersed distribution and a potential size of around 10 nm for biological implementations (Bartucci et al., 2020).

### 3.2. FTIR measurement

Fig. 2 depicts the FTIR spectrum for synthesized $SnO_2$ NPs in the wavenumber region of 4000–400 $cm^{-1}$. The strong absorption peaks at 1635 $cm^{-1}$ and 3476 $cm^{-1}$ attribute to the stretching of H–O–H and O–H bonds, respectively deduced from water molecules (Garg et al., 2020). One broader absorption peak is also visible in the spectrum at 649 $cm^{-1}$, corresponding to the stretching vibration of the O–Sn–O bond (Garg et al., 2020; Sery et al., 2022).

This data showed the purity and the lack of crystal lattice defects or disorders in synthesized $SnO_2$ NPs (Garg et al., 2020; Sery et al., 2022).

### 3.3. XRD analysis

The XRD pattern of the synthesized $SnO_2$ NPs is shown in Fig. 3. The

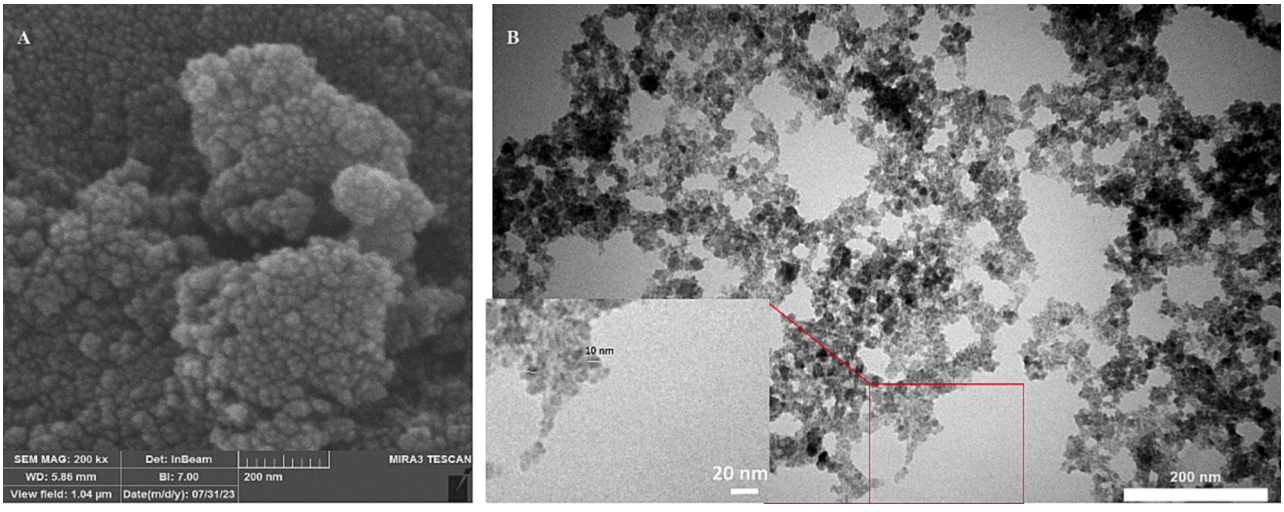


**Fig. 1.** SEM (A) and TEM (B) imaging of synthesized $SnO_2$ NPs through the combination of solvent polarity reduction and sonochemical method.

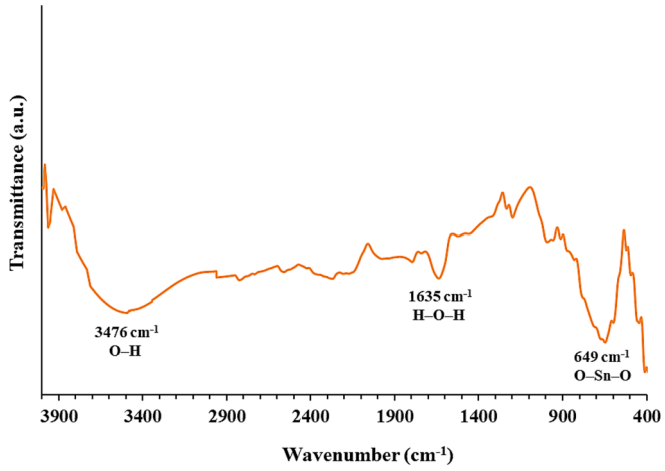


**Fig. 2.** FTIR spectrum of synthesized $SnO_2$ NPs.

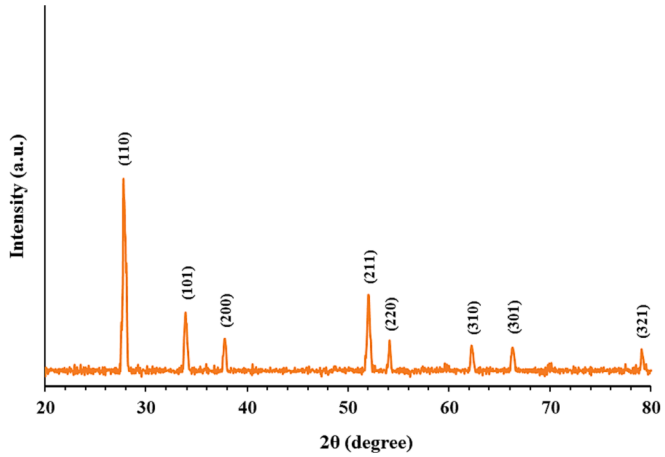


**Fig. 3.** XRD pattern of synthesized $SnO_2$ NPs.

peaks at 2θ values of 27.75°, 33.80°, 37.80°, 52.05°, 54.15°, 62.35°, 66.40°, and 79.01° can be attributed to (110), (101), (200), (211), (220), (310), (301), and (321) plans, respectively (Patil et al., 2012; Sery et al., 2022). A matching of the detected and standard (*hkl*) planes proved that the particle is of $SnO_2$ with a tetragonal system of rutile-like structure, which is in good agreement with the literature values (JCPDS, PDF file No 41–1445, space group P42/MNM, lattice parameters a = 4.7420 Å and c = 3.1900 Å) (Sery et al., 2022).

No other detectable XRD peaks were observed, revealing the high purity of the synthesized $SnO_2$ NPs (Sery et al., 2022). Also, XRD patterns of $SnO_2$ NPs demonstrated high peak intensities, suggesting ideal crystallinity and crystallite-size developments (Sery et al., 2022), which is consistent with the NP size observed by TEM analysis. Also, slight broad peaks were detected for synthesized $SnO_2$ NP samples corroborating the generation of fine nanosized samples (Sery et al., 2022). Therefore, it can be assumed that the sonication of the solution provides us with a high probability of synthesizing particles in the nanometer size.

### 3.4. Hydrodynamic radius and charge studies

DLS study was also done to measure the hydrodynamic radius and zeta potential values of the synthesized $SnO_2$ NPs. Fig. 4 A shows the hydrodynamic size of the dispersed synthesized $SnO_2$ NPs in solution determined by DLS which was found to be ranged between 34 and 60 nm with an average size of 43.93 nm. The differences in determined size

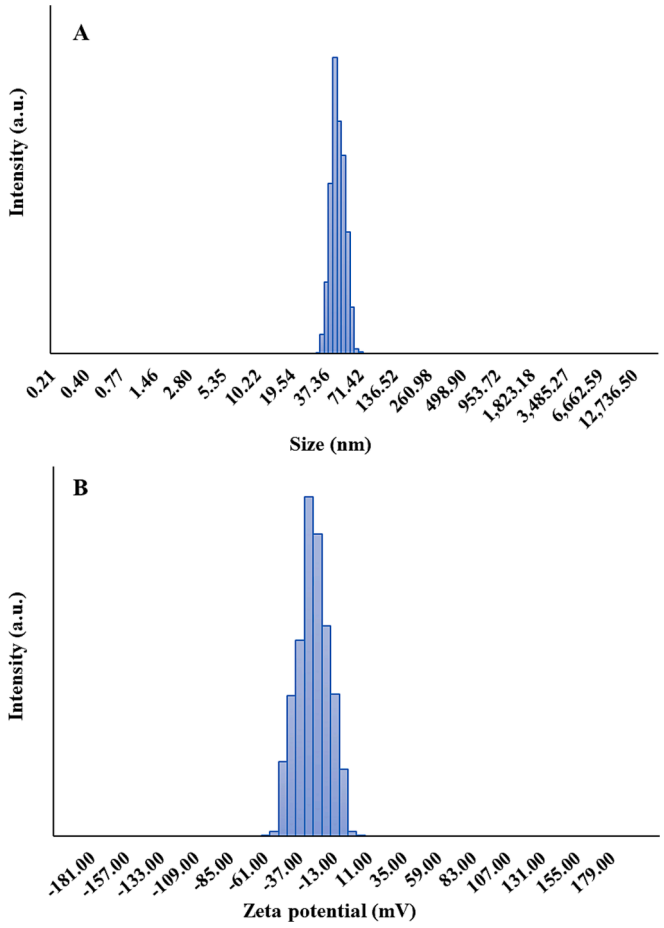


**Fig. 4.** DLS (A) and zeta potential (B) analyses of synthesized $SnO_2$ NPs.

between TEM and DLS techniques could be associated with the slight agglomeration of NPs in the solution. However, a monodisperse distribution of synthesized $SnO_2$ NPs was detected in Fig. 4A, which could be due to the cavitation process induced by the nonchemical approach, which results in large NPs breaking up into homogenous small particles and their slight aggregation (Barbhuiya et al., 2022).

Fig. 4B depicts that the average zeta potential of synthesized $SnO_2$ NPs was −31.00 mV. This strong negative value indicates an apparent particle repulsion, corresponding to the stability of NPs (Manimaran, Muthuvel,and Said, 2023). Generally, zeta potential reveals how electrostatic forces determine the strength of repulsion forces between neighboring NPs. Following the adsorption of $OH^-$ ions on the surface of NPs, their zeta potential values become negative, inhibiting the strong NP aggregation and maintaining the colloidal stability (Manimaran, Muthuvel,and Said, 2023; Srivastava and Mukhopadhyay, 2014).

### 3.5. $SnO_2$ NPs interaction with cells

The anticancer activity of synthesized $SnO_2$ NPs on U-2OS human osteosarcoma cells was evaluated by using the MTT assay. As depicted in Fig. 5A, treatment with synthesized $SnO_2$ NPs for 24 h significantly decreased the proliferation of U-2OS cells in a concentration-dependent fashion in comparison to control cells (*P < 0.05, **P < 0.01, ***P < 0.001), while the growth of human normal osteoblasts NHOst cells (Fig. 5B) was much less influenced by the synthesized $SnO_2$ NPs at the same studied concentrations.

Therefore, the $IC_{50}$ concentration of synthesized $SnO_2$ NPs on U-2OS human osteosarcoma cells was determined to be about 15.50 μg/mL at 24 h.

A previous study has shown that biosynthesized $SnO_2$ NPs with

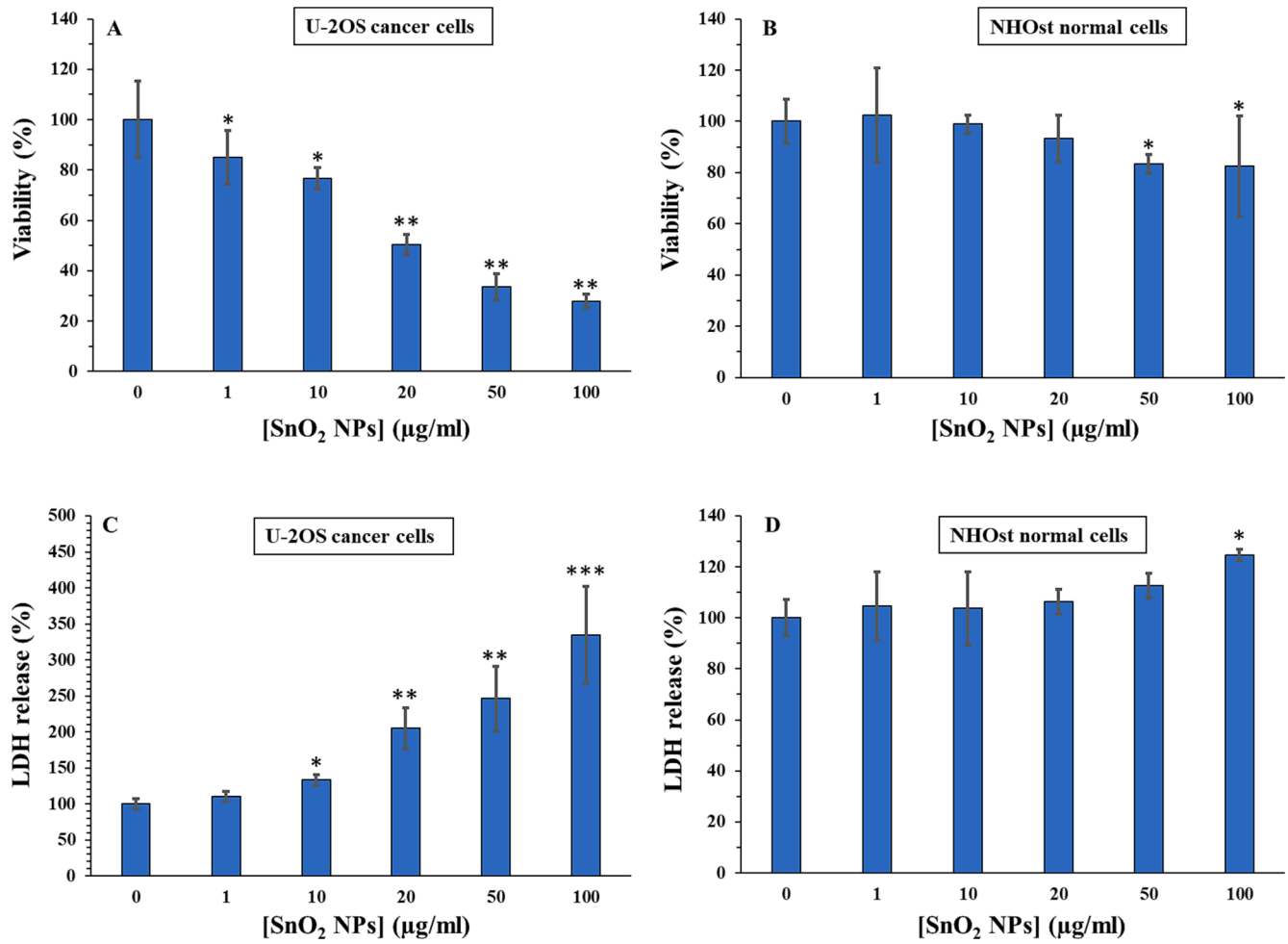


**Fig. 5.** Cytotoxic effects of $SnO_2$ NPs against U-2OS human osteosarcoma cells (A) and human normal osteoblasts NHOst cells (B) determined by MTT assay. Membrane leakage induced by $SnO_2$ NPs in U-2OS human osteosarcoma cells (C) and human normal osteoblasts NHOst cells (D) determined by LDH assay. All experiments were done after 24 h incubation of cells with $SnO_2$ NPs. *P < 0.05, ** P < 0.01, *** P < 0.001 relative to control. Data were presented as mean ± SD of three experiments.

particle size distribution ranging between 5 and 10 nm had significant antiproliferative effects against colorectal and lung cancer cells with $IC_{50}$ values of 165–208 µg/mL and 138–187 µg/mL, respectively (Tammina et al., 2017). Additionally, Hanna et al. (Hanna and R. Saad 2021) reported that the calculated $IC_{50}$ value for the sol–gel synthesized $SnO_2$ NPs with a size of around 79 nm against SKOV3 human ovarian cancer cells, was 47.87 µg/mL at 24 h incubation. However, Ahamed et al. (Ahamed et al., 2018) reported that the sol–gel synthesized $SnO_2$ NPs with a size of about 21 nm did not induce cytotoxicity in MCF-7 breast cancer cells up to the concentration 50 µg/mL at 24 and 48 h. Therefore, several parameters may play a key role in the NP-induced cytotoxicity such as the physicochemical properties of NPs, type of cancer or normal cells, and experimental procedures.

LDH enzyme release from cytoplasm into cell culture medium can be appointed as a useful marker of damage to cell membrane integrity (Ahamed et al., 2018). Higher levels of LDH enzyme activity in cell culture media reveal the higher damage of cell membranes induced by NP exposure (Ifijen et al., 2023). We also found that synthesized $SnO_2$ NPs prompted LDH leakage in U-2OS human osteosarcoma cells in a concentration-dependent manner (Fig. 5C), whereas these NPs did not induce a significant LDH release in normal human osteoblast, NHOst, below 100 µg/mL at 24 h (Fig. 5D). Altogether, these data proved that $SnO_2$ NPs show potential to trigger concentration-dependent cytotoxicity in the U-2OS cell line. Our findings are consistent with recent reports demonstrating $SnO_2$ NPs' anticancer effects in several cancer cells (Ahamed et al., 2018; Ahmadabad et al., 2021; Ifijen et al., 2023).

### 3.6. *$SnO_2$ NPs induced oxidative stress in U-2OS human osteosarcoma cells*

Induction of oxidative stress through inhibition of antioxidant enzyme activities and depletion of non-enzymatic antioxidants are the most common pathways through which NPs stimulate apoptosis in cancer cells (Akhtar et al., 2012; Rayzah et al., 2023). To maintain the redox balance in cells, antioxidant defense and strict control over the generation of free radicals are essential (Rayzah et al., 2023). The GSH, SOD, and CAT are serving as strong antioxidant molecules in protecting cells from oxidative stress prompted by ROS and other free radicals (Rayzah et al., 2023). Antioxidant enzymes, SOD and CAT, are crucial for shielding cells from the damaging effects of free radicals. GSH plays a crucial role in inhibiting lipid peroxidation (Rayzah et al., 2023). Because cancer cells can express antioxidant molecules, they are able to eliminate the excessive generation of ROS, extending their survival half-life through preventing apoptosis. On the other hand, elevated oxidative stress in cancerous cells may initiate anti-tumorigenic signaling cascades, resulting in tumor cell death (Zeng et al., 2023; Tuli, Kaur, et al. 2023).

Therefore, the oxidant and antioxidant levels were examined in the U-2OS cell line treated with $SnO_2$ NPs with a concentration of 15.50 µg/mL at 24 h. ROS (Fig. 6A) and MDA (Fig. 6B) levels were assessed as

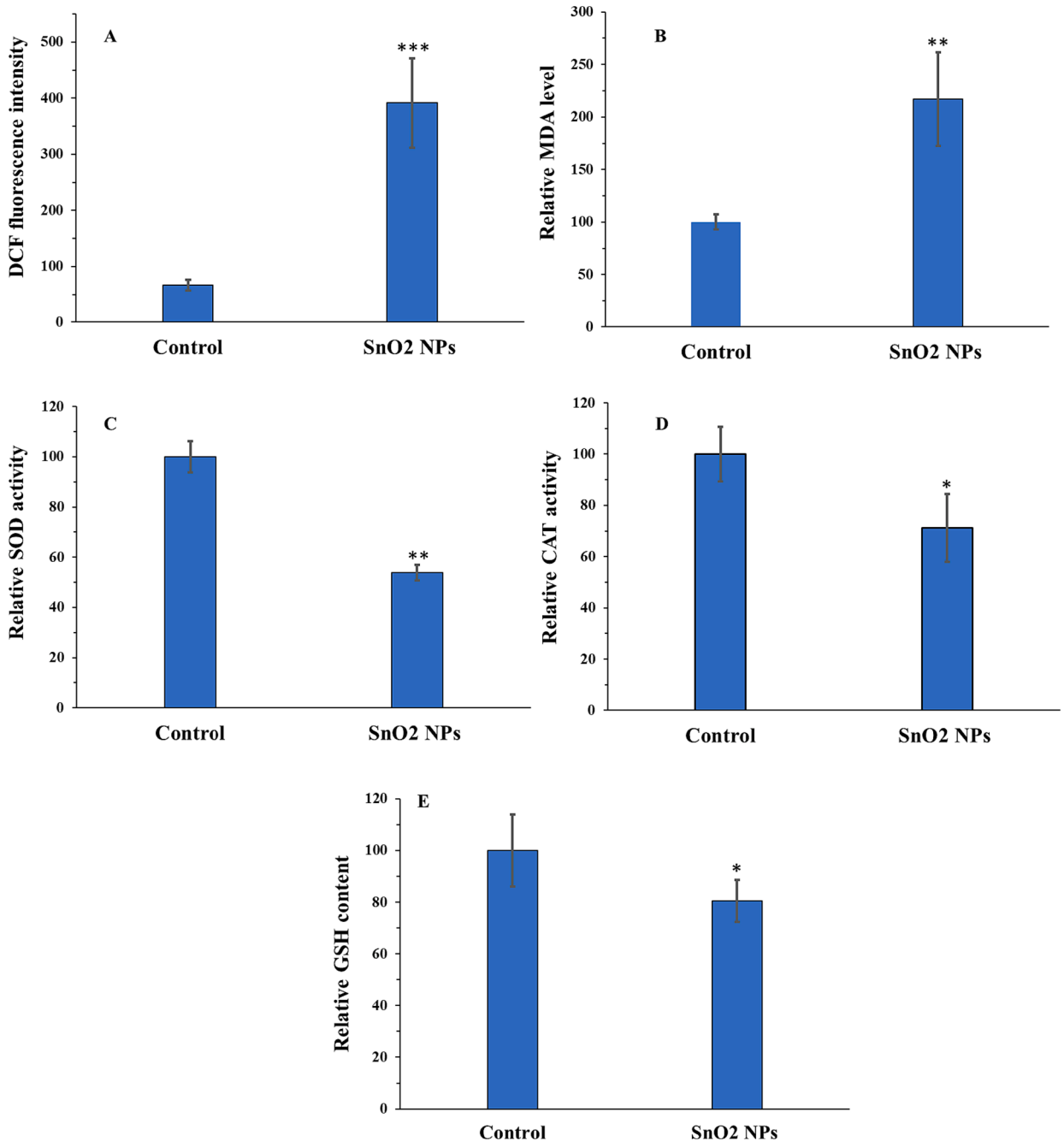


**Fig. 6.** Oxidative stress induction of $SnO_2$ NPs in U-2OS human osteosarcoma cells determined by ROS assay (A), MDA assay (B), SOD assay (C), CAT assay (D), and GSH assay (E). All experiments were done after 24 h incubation of cells with $SnO_2$ NPs. *P < 0.05, ** P < 0.01, *** P < 0.001 relative to control. Data were presented as mean ± SD of three experiments.

main biomarkers of oxidative stress, whereas antioxidant status was assessed by analyzing the SOD (Fig. 6C) and CAT (Fig. 6D) activities as well as GSH content (Fig. 6E). The obtained data displayed that oxidant (ROS and MDA) levels were higher in $SnO_2$ NPs-treated cancer cells compared to negative control cells (Fig. 6A and B).

Furthermore, CAT and SOD activities as well as the GSH content were remarkably reduced by the $IC_{50}$ concentration of $SnO_2$ NPs (Fig. 6C-E). These findings indicated that $SnO_2$ NP treatment collapses the antioxidant system of the cells while increasing the ROS and MDA levels, thereby accelerating oxidative stress-manipulated cell death in U-2OS human osteosarcoma cells. These data are in good agreement with a study reported by Ahamed et al. (Ahamed et al., 2018), indicating that $SnO_2$ NPs could induce oxidative stress-mediated anticancer effects through deregulation of enzymatic and non-enzymatic oxidants.

### 3.7. *$SnO_2$ NPs activated both intrinsic and extrinsic signaling pathways*

There are two possible ways for NPs to trigger apoptotic cell death: intrinsic or extrinsic pathways (Tuli,Joshi,et al., 2023). Intrinsic mechanisms of apoptosis are activated by non-receptor mediated stimuli that trigger the disruption of several mediators such as MMP, Bax/Bcl-2 ratio, and caspase-9 activity to stimulate apoptosis, whereas extrinsic apoptotic cell death is initiated upon the interaction of anticancer drugs with transmembrane receptors and activation of caspase-8 (Lossi, 2022; Fulda and Debatin, 2006). Metal NPs are potential candidates to induce apoptotic cell death in different types of cancers, including bone, brain,

blood, liver, and so on (Tuli,Joshi,et al., 2023). Especially, functionalized $SnO_2$ NPs have been observed to promote anticancer activity in human ovarian cancer cells by overexpression of Bax, and cleaved caspase-3 (Hanna and R. Saad, 2021). In cervical cancer HeLa cells, cell $SnO_2$ NP treatment was shown to deregulate the Bax/Bcl-2 mRNA ratio (Bazsefidpar et al., 2021). Guo et al. explored the downregulation of PI3K/Akt/mTOR/Bax/Bcl-2 in $SnO_2$ NPs- treated breast cancer cells, leading to apoptotic cell death (Guo et al., 2021). Similarly, Jiang et al. (Jiang et al., 2022) observed the apoptotic effect of biosynthesized $SnO_2$-sodium alginate-polyethylene glycol-carvacrol NPs in esophagus squamous cells cancer via upregulation of Bax and caspase 3. Therefore, in this study, for 24 h to assess if synthesized $SnO_2$ NP solution at the $IC_{50}$ concentration (15.50 μg/mL) could induce apoptotic effects in U-2OS human osteosarcoma cells via intrinsic or extrinsic pathways, MMP, qRT-PCR, and caspase activity assays were performed.

As determined by the decreased ratio of red to green fluorescence by JC-1 staining, incubation with the $SnO_2$ NP solution at the $IC_{50}$ concentration (15.50 μg/mL) for 24 h significantly reduced MMP in U-2OS human osteosarcoma cells, compared with negative treated cells (Fig. 7A). Furthermore, All the caspase activities under study found to be increased (Fig. 7B-D) following incubation of U-2OS cells with 15.50 μg/mL $SnO_2$ NPs at 24 h, compared to control cells.

Additionally, the upregulated levels of Bax mRNA, caspase-9 mRNA, caspase-8 mRNA and caspase-3 mRNA, and the reduced level of Bcl-2 mRNA were observed in U-2OS human osteosarcoma cells following incubation with 15.50 μg/mL $SnO_2$ NPs at 24 h (Fig. 7E). These results confirmed the activation of both intrinsic and extrinsic apoptosis signaling pathways by $SnO_2$ NPs in the U-2OS cells. Using leukemia

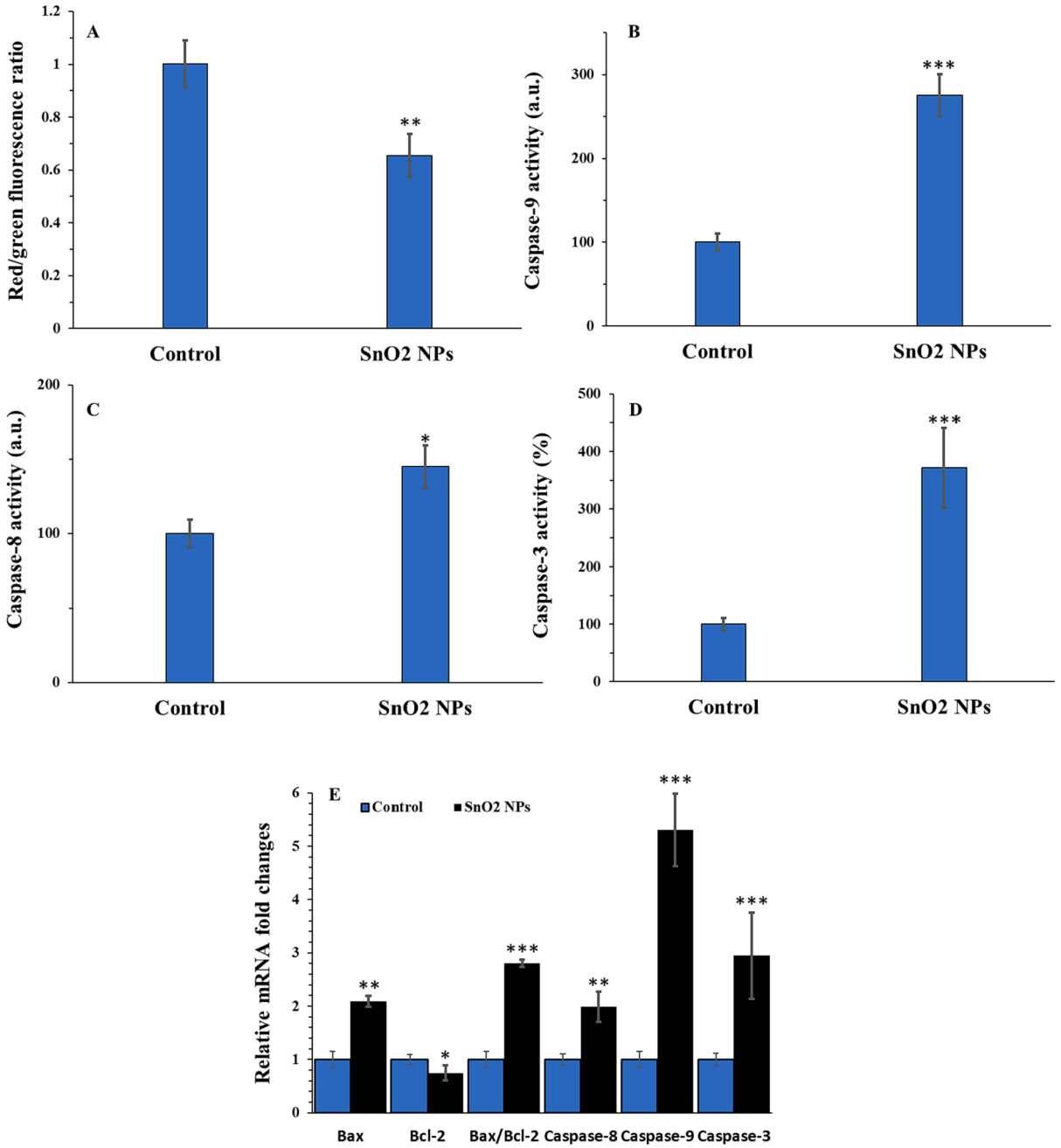


**Fig. 7.** Apoptosis induction of $SnO_2$ NPs in U-2OS human osteosarcoma cells determined by different assays. MMP assay (A), caspase-9 activity assay (B), caspase-8 activity assay (C), caspase-3 activity assay (D), and qRT-PCR assay (E). All experiments were done after 24 h incubation of cells with $SnO_2$ NPs. *P < 0.05, ** P < 0.01, *** P < 0.001 relative to control. Data were presented as mean ± SD of three experiments.

K562 cells, Ahmadabad et al. (Ahmadabad et al., 2021) showed that synthesized $SnO_2$ NPs through hydrothermal method with a size of 60 nm triggered overexpression of caspase-9, −8, −3 and Bax/Bcl2 mRNA ratio. However, the main drawback of this study was the heterogenous distribution of synthesized NPs in solvent as determined by the DLS study.

## 4. Conclusion

In conclusion, $SnO_2$ NPs with an average size of around 10 nm were produced via a combination of solvent polarity reduction and sono-chemical route and well-characterized by different techniques. Then, we demonstrated that synthesized $SnO_2$ NPs, concentration-dependently mitigated the proliferation of U-2OS human osteosarcoma cells through induction of membrane leakage, oxidative stress as well as apoptosis mediated by both intrinsic and extrinsic signaling pathways. These outcomes indicated that synthesized $SnO_2$ NPs could be a promising novel therapeutic nanostructure for the treatment of osteosarcoma. Further investigations are required to discover whether $SnO_2$ NPs can combine with different chemotherapeutics.

## CRediT authorship contribution statement

**Ruxin Ruan:** Methodology, Writing – original draft, Visualization, Resources. **Rui Chen:** Methodology, Writing – original draft, Visualization, Resources. **Huaixi Yu:** Conceptualization, Supervision, Writing – review & editing.

## Declaration of competing interest

The authors declare that they have no known competing financial interests or personal relationships that could have appeared to influence the work reported in this paper.

## Acknowledgments

The authors would like to express their deepest gratitude to the corresponding institutions for the technical support for this study

## References

Ahamed, M., Akhtar, M.J., Majeed Khan, M.A., Alhadlaq, H.A., 2018. Oxidative stress mediated cytotoxicity of tin (IV) oxide (SnO2) nanoparticles in human breast cancer (MCF-7) cells. Colloids Surf. B Biointerfaces 172, 152–160.

Ahmadabad, L.E., Kalantari, F.S., Liu, H., Hasan, A., Gamasaee, N.A., Edis, Z., Attar, F., Ale-Ebrahim, M., Rouhollah, F., Babadaei, M.M.N., 2021. Hydrothermal method-based synthesized tin oxide nanoparticles: Albumin binding and antiproliferative activity against K562 cells. Mater. Sci. Eng. C 119, 111649.

Akhtar, Mohd Javed, Ahamed, Maqusood, Sudhir Kumar, M.A., Khan, Majeed, Ahmad, Javed, Alrokayan, Salman A., 2012. Zinc oxide nanoparticles selectively induce apoptosis in human cancer cells through reactive oxygen species. Int. J. Nanomed. 845–857.

Alrushaid, N., Khan, F.A., Al-Suhaimi, E.A., Elaissari, A., 2023. Nanotechnology in cancer diagnosis and treatment. Pharmaceutics 15, 1025.

Bandyopadhyay, A., Roy, B., Shaw, P., Mondal, P., Mondal, M.K., Chowdhury, P., Bhattacharya, S., Chattopadhyay, A., 2020. Cytotoxic effect of green synthesized silver nanoparticles in MCF7 and MDA-MB-231 human breast cancer cells in vitro. Nucleus 63, 191–202.

Barbhuiya, R.I., Singha, P., Asaithambi, N., Singh, S.K., 2022. Ultrasound-assisted rapid biological synthesis and characterization of silver nanoparticles using pomelo peel waste. Food Chem. 385, 132602.

Bartucci, R., Paramanandana, A., Boersma, Y.L., Olinga, P., Salvati, A., 2020. Comparative study of nanoparticle uptake and impact in murine lung, liver and kidney tissue slices. Nanotoxicology 14, 847–865.

Bazsefidpar, P., Koochakkhani, S., Inchehsablagh, B.R., Eftekhar, E., Aliasgari, E., 2021. Tin (IV) oxide (SnO2) nanoparticles inhibit the viability of cervical cancer HeLa cells through induction of apoptosis. Journal of Reports in Pharmaceutical Sciences 10, 225.

Bonjoch, Nuria Pedrol, and Pilar Ramos Tamayo. 2001. 'Protein content quantification by Bradford method.' in, *Handbook of plant ecophysiology techniques* (Springer).

Choudhari, A., Bhanvase, B.A., Saharan, V.K., Salame, P.H., Hunge, Y., 2020. Sonochemical preparation and characterization of rGO/SnO2 nanocomposite: Electrochemical and gas sensing performance. Ceram. Int. 46, 11290–21126.

Deosarkar, M.P., Pawar, S.M., Sonawane, S.H., Bhanvase, B.A., 2013. Process intensification of uniform loading of SnO2 nanoparticles on graphene oxide nanosheets using a novel ultrasound assisted in situ chemical precipitation method. Chem. Eng. Process. 70, 48–54.

Ferrari, M., 2005. Cancer nanotechnology: opportunities and challenges. Nat. Rev. Cancer 5, 161–171.

Fulda, S., Debatin, K.-M., 2006. Extrinsic versus intrinsic apoptosis pathways in anticancer chemotherapy. Oncogene 25, 4798–4811.

Garg, Vijay, Harsh Sharma, Divya Rehani, Renu Kumari, Vipin Kumar, Manoj Kumar Tiwari, Shailesh Narain Sharma, and Manish Saxena. 2020. 'Synthesis and Characterization of Temperature Controlled SnO2 Nanoparticles by Solid-state Reaction Method'.

Guo, Y., Zhao, Y., Zhao, X., Song, S., Qian, B., 2021. Exploring the anticancer effects of tin oxide nanoparticles synthesized by pulsed laser ablation technique against breast cancer cell line through downregulation of PI3K/AKT/mTOR signaling pathway. Arab. J. Chem. 14, 103212.

Hanna, D.H., Saad, G.R., 2021. Induction of mitochondria mediated apoptosis in human ovarian cancer cells by folic acid coated tin oxide nanoparticles. PLoS One 16, e0258115.

Hussain, M.H., Bakar, N.F.A., Mustapa, A.N., Low, K.-F., Othman, N.H., Adam, F., 2020. Synthesis of various size gold nanoparticles by chemical reduction method with different solvent polarity. Nanoscale Res. Lett. 15, 1–10.

Ifijen, I.H., Ikhuoria, E.U., Omorogbe, S.O., Anegbe, B., Jonathan, E.M., Chikaodili, D.I., 2023. Chemical, plant and microbial mediated synthesis of tin oxide nanoparticles: antimicrobial and anticancer potency. Braz. J. Chem. Eng. 1–27.

Jiang, G., Mohideen, A.P., Seshadri, V.D., Rengarajan, T., 2022. Biosynthesized tin oxide-sodium alginate-polyethylene glycol-carvacrol nanocomposite shows anticancer activity on esophagus squamous carcinoma cells. Process Biochem. 121, 403–412.

Karunakaran, C., Sakthi Raadha, S., Gomathisankar, P., 2013. Microstructures and optical, electrical and photocatalytic properties of sonochemically and hydrothermally synthesized SnO2 nanoparticles. J. Alloy. Compd. 549, 269–275.

Li, Z., Zhuang, T., Dong, J., Wang, L., Xia, J., Wang, H., Cui, X., Wang, Z., 2021. Sonochemical fabrication of inorganic nanoparticles for applications in catalysis. Ultrason. Sonochem. 71, 105384.

Liang, C.Z., Zhang, J.K., Shi, Z., Liu, B., Shen, C.Q., Tao, H.M., 2012. Matrine induces caspase-dependent apoptosis in human osteosarcoma cells in vitro and in vivo through the upregulation of Bax and Fas/FasL and downregulation of Bcl-2. Cancer Chemother. Pharmacol. 69, 317–331.

Lossi, L., 2022. The concept of intrinsic versus extrinsic apoptosis. Biochem. J 479, 357–384.

Low, S.S., Yew, M., Lim, C.N., Chai, W.S., Low, L.E., Manickam, S., Tey, B.T., Show, P.L., 2022. Sonoproduction of nanobiomaterials–A critical review. Ultrason. Sonochem. 82, 105887.

Manimaran, M., Muthuvel, A., Said, N.M., 2023. Microwave-assisted green synthesis of SnO2 nanoparticles and their photocatalytic degradation and antibacterial activities. Nanotechnology for Environmental Engineering 8, 413–423.

Patil, G.E., Kajale, D.D., Gaikwad, V.B., Jain, G.H., 2012. Preparation and characterization of SnO2 nanoparticles by hydrothermal route. International Nano Letters 2, 17.

Punzo, F., Tortora, C., Di Pinto, D., Manzo, I., Bellini, G., Casale, F., Rossi, F., 2017. Anti-proliferative, pro-apoptotic and anti-invasive effect of EC/EV system in human osteosarcoma. Oncotarget 8, 54459.

Rayzah, M., Elderdery, A.Y., Alzerwi, N.A.N., Alzahrani, B., Alsrhani, A., Alsultan, A., Idrees, B., Rayzah, F., Bakhsh, Y., Alzahrani, A.M., 2023. Syzygium cumini (L.) Extract-Derived Green Titanium Dioxide Nanoparticles Induce Caspase-Dependent Apoptosis in Hepatic Cancer Cells. Plants 12, 3174.

Rehman, S., Asiri, S.M., Khan, F.A., Rabindran Jermy, B., Ravinayagam, V., Alsalem, Z., Jindan, R.A., Qurashi, A., 2020. Anticandidal and in vitro anti-proliferative activity of sonochemically synthesized indium tin oxide nanoparticles. Sci. Rep. 10, 3228.

Ritter, J., Bielack, S.S., 2010. Osteosarcoma. Ann. Oncol. 21.

Saini, P., Saha, S.K., Roy, P., Chowdhury, P., Babu, S.P.S., 2016. Evidence of reactive oxygen species (ROS) mediated apoptosis in Setaria cervi induced by green silver nanoparticles from Acacia auriculiformis at a very low dose. Exp. Parasitol. 160, 39–48.

Sery, A.A., Walied, A.A., Mohamed, F.F., Hammad, M.M.H.K., Farag, H.K., 2022. Synthesis of pure and doped SnO2 and NiO nanoparticles and evaluation of their photocatalytic activity. Mater. Chem. Phys. 275, 125190.

Shabatina, T.I., Vernaya, O.I., Shimanovskiy, N.L., Melnikov, M.Y., 2023. Metal and Metal Oxides Nanoparticles and Nanosystems in Anticancer and Antiviral Theragnostic Agents. Pharmaceutics 15, 1181.

Srivastava, N., Mukhopadhyay, M., 2014. Biosynthesis of SnO2 nanoparticles using bacterium Erwinia herbicola and their photocatalytic activity for degradation of dyes. Ind. Eng. Chem. Res. 53, 13971–111399.

Tammina, S.K., Mandal, B.K., Ranjan, S., Dasgupta, N., 2017. Cytotoxicity study of Piper nigrum seed mediated synthesized SnO2 nanoparticles towards colorectal (HCT116) and lung cancer (A549) cell lines. J. Photochem. Photobiol. B Biol. 166, 158–168.

Tuli, H.S., Joshi, R., Kaur, G., Garg, V.K., Sak, K., Varol, M., Kaur, J., Alharbi, S.A., Alahmadi, T.A., Aggarwal, D., 2023a. Metal nanoparticles in cancer: from synthesis and metabolism to cellular interactions. Journal of Nanostructure in Chemistry 13, 321–348.

Tuli, H.S., Kaur, J., Vashishth, K., Sak, K., Sharma, U., Choudhary, R., Behl, T., Singh, T., Sharma, S., Saini, A.K., 2023b. Molecular mechanisms behind ROS regulation in

cancer: A balancing act between augmented tumorigenesis and cell apoptosis. Arch. Toxicol. 97, 103–120.
Zeng, W., Long, X., Liu, P.-S., Xie, X., 2023. The interplay of oncogenic signaling, oxidative stress and ferroptosis in cancer. Int. J. Cancer.
Zhu, J., Zhonghua, L.u., Aruna, S.T., Aurbach, D., Gedanken, A., 2000. Sonochemical synthesis of SnO2 nanoparticles and their preliminary study as Li insertion electrodes. Chem. Mater. 12, 2557–2566.